Chapter 14

Renal pH Imaging Using Chemical Exchange Saturation Transfer (CEST) MRI: Basic Concept

Dario Livio Longo, Pietro Irrera, Lorena Consolino, Phillip Zhe Sun, and Michael T. McMahon

Abstract

Magnetic Resonance Imaging (MRI) has been actively explored in the last several decades for assessing renal function by providing several physiological information, including glomerular filtration rate, renal plasma flow, tissue oxygenation and water diffusion. Within MRI, the developing field of chemical exchange saturation transfer (CEST) has potential to provide further functional information for diagnosing kidney diseases. Both endogenous produced molecules as well as exogenously administered CEST agents have been exploited for providing functional information related to kidney diseases in preclinical studies. In particular, CEST MRI has been exploited for assessing the acid-base homeostasis in the kidney and for monitoring pH changes in several disease models. This review summarizes several CEST MRI procedures for assessing kidney functionality and pH, for monitoring renal pH changes in different kidney injury models and for evaluating renal allograft rejection.

This chapter is based upon work from the COST Action PARENCHIMA, a community-driven network funded by the European Cooperation in Science and Technology (COST) program of the European Union, which aims to improve the reproducibility and standardization of renal MRI biomarkers. This introduction chapter is complemented by two separate chapters describing the experimental procedure and data analysis.

Key words Magnetic resonance imaging (MRI), Kidney, Mice, Rats, pH, Iopamidol, Chemical exchange saturation transfer (CEST), Acute kidney injury, Ischemia–reperfusion injury, Renal damage

1 Introduction

Renal dysfunction is recognized as a significant health problem originating from a variety of causes leading to acute or chronic kidney diseases. Predisposition to acute kidney injury and premature mortality are frequent outcomes for chronic kidney diseases [1]. Moreover, according to the Global Burden of Disease 2013 study, the age-standardized death rates for chronic kidney diseases showed one of the highest increases in the last two decades [2]. Therefore, reliable and early diagnosis of acute and chronic kidney diseases is needed to preserve renal functionality and

Andreas Pohlmann and Thoralf Niendorf (eds.), *Preclinical MRI of the Kidney: Methods and Protocols*, Methods in Molecular Biology, vol. 2216, https://doi.org/10.1007/978-1-0716-0978-1_14, © The Author(s) 2021

improve patients' outcome. Despite these premises, current clinical evaluation of renal function is still based on measurement of serum creatinine, which is well known to have several limitations. In fact, an elevated serum creatinine concentration is only discovered at late stages of the disease when renal functionality is already compromised. Therefore, novel noninvasive imaging approaches are needed for a more accurate and early diagnosis of renal physiology. Magnetic resonance imaging (MRI) has been exploited for tissue anatomic imaging, owing to the high spatial resolution and lack of ionizing radiation. In research, novel MRI techniques have been investigated for assessing multiple functional parameters of the kidneys, including perfusion, filtration, oxygenation and tissue elasticity [3–11]. Several reviews covering the role of these MRI approaches for assessing renal functionality have been published [12–15]. This additional information should enable a better characterization of acute and chronic kidney diseases in comparison to standard urine and serum-based assays.

Recently, Chemical Exchange Saturation Transfer (CEST) MRI has emerged as a novel approach for functional and molecular imaging with great promise for clinical translation [16–18]. In addition, CEST MRI pH imaging has emerged as a valuable approach for assessing extracellular pH values in several tissues, including kidneys and tumors, providing the highest accuracy and spatial resolution achievable so far [19]. Owing to the key role of the kidneys in maintaining the acid-base homeostasis, CEST MRI pH mapping has emerged as a novel and promising approach in monitoring kidney functionality.

In this chapter, we will address the basic concept and the developments of renal CEST pH imaging with the emphasis on kidney disease models in rodents.

This introduction chapter is complemented by two separate chapters describing the experimental procedure and data analysis, which are part of this book.

This chapter is part of the book Pohlmann A, Niendorf T (eds) (2020) Preclinical MRI of the Kidney—Methods and Protocols. Springer, New York.

2 Measurement Concept

2.1 Basic Concept of Chemical Exchange Saturation Transfer (CEST) Imaging

CEST is a new technique that enables the indirect detection of molecules possessing mobile protons in exchange with water [20]. Because of this, CEST makes MRI sensitive to endogenous or exogenous molecules that possess suitable protons [21–32]. The generation of contrast is based on a selective irradiation with a radiofrequency pulse at the specific absorption frequency of the exchanging proton, followed by a subsequent transfer, due to chemical exchange with bulk water, of the saturated signal. Upon the application of a long saturation RF (radiofrequency) pulse, the

water signal decreases, allowing the amplification of the labeled protons from the molecule to water. As a consequence, low concentration molecules can be specifically and indirectly detected, owing to the frequency selective irradiation of their mobile proton pool(s) [33–38].

2.2 CEST Contrast Agents for Imaging Kidneys and Mapping pH

Several classes of CEST contrast agents can be used as pH responsive agents and exploited for in vivo experiments.

2.2.1 Diamagnetic CEST Agents

Several molecules, including natural occurring molecules, possess exchangeable protons that can be indirectly detected within the CEST approach [39]. Most of these labile protons have chemical exchange rates that show a strong pH dependence. Hence differences in CEST contrast can be exploited for assessing the pH of the solution where they are dissolved. Due to the concomitant contribution of concentration and exchange rate to the observed CEST contrast, several approaches have been proposed to rule out the concentration term, based on the ratiometric method, that is, taking the ratio of the observed contrast, providing accurate pH readouts [40, 41]. Most of the pH responsive diamagnetic molecules investigated so far in vivo are iodinated contrast agents used for radiographic procedures, since they have been used in the last 40 years in clinical examinations owing to their high safety profiles [42, 43]. The presence of amide groups in their chemical structure allow them to be exploited as CEST MRI contrast agents, upon selective irradiation of the mobile proton pool [44].

Among the radiographic contrast media, Iopamidol (Isovue®, Bracco Imaging, Italy) (Fig. 1) was the first agent exploited for mapping pH thanks to the presence of two amide groups with different resonance frequencies, at 4.2 ppm and at 5.5 ppm, respectively, that can be selectively irradiated [45–47]. This chemical peculiarity led to the development of a ratiometric approach based on the ratio of the CEST effects at these two frequencies to provide accurate pH measurements. In vitro experiments showed a high pH responsiveness within the physiological range and accurate pH measurements (Fig. 2a, b). Following intravenous administration, it can provide selective contrast at specific frequency offsets and from the ratio of these two parametric maps it is possible to measure renal pH map (Fig. 2c–f). To validate the approach and test the pH-responsiveness of the agent, induced alkalinisation or acidification of urine was obtained in mice upon providing acidic or alkaline drinking water for a week. For control mice, mean pH values calculated for cortex, medulla and calyx regions were: 7.0 ± 0.11; 6.85 ± 0.15 and 6.6 ± 0.20, respectively. In mice drinking acidic water a significant acidification of renal pH values was obtained. Conversely, a marked increase of renal pH values was

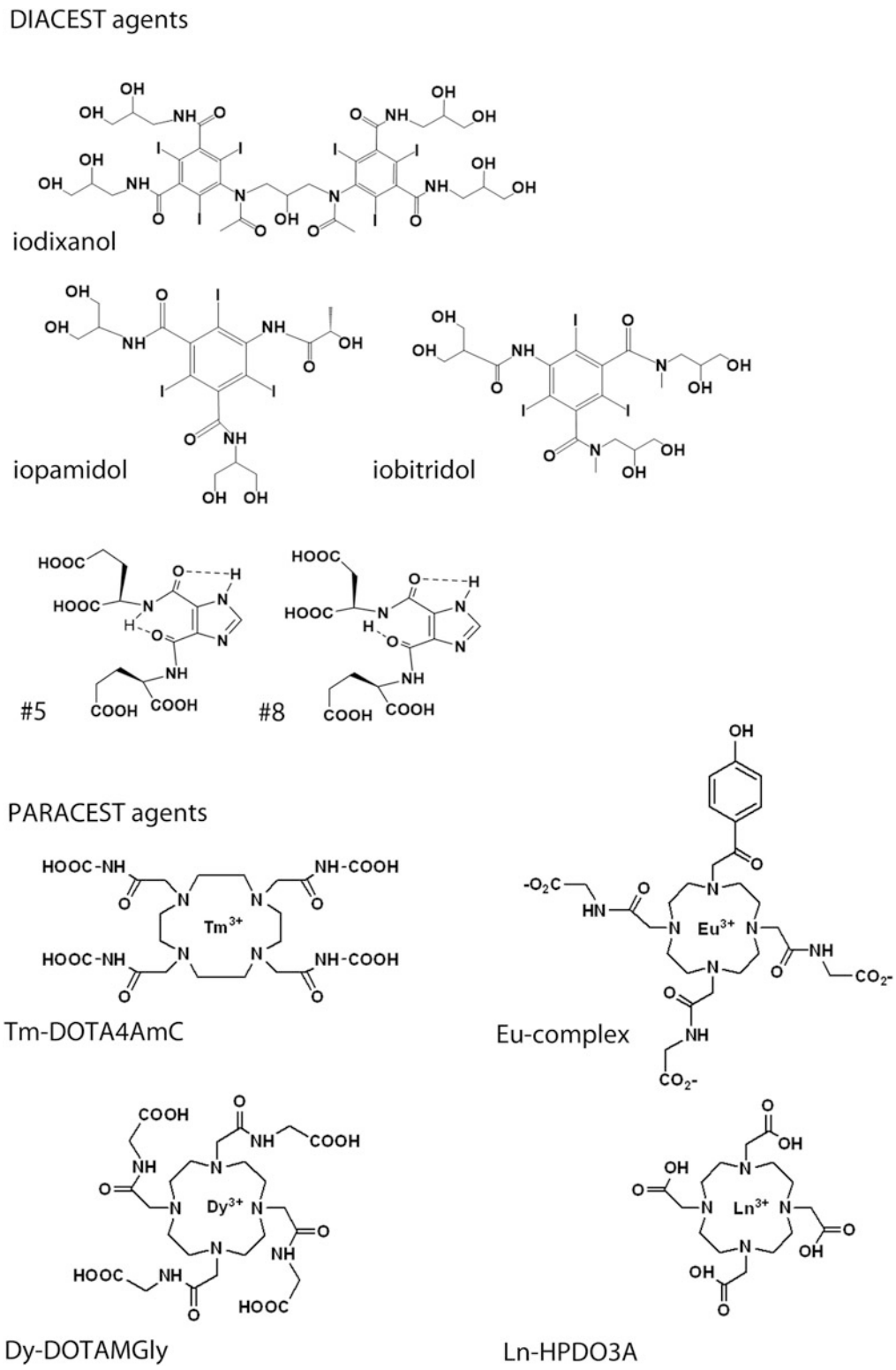

Fig. 1 Chemical structures of the reported pH-responsive CEST agents investigated for renal pH mapping

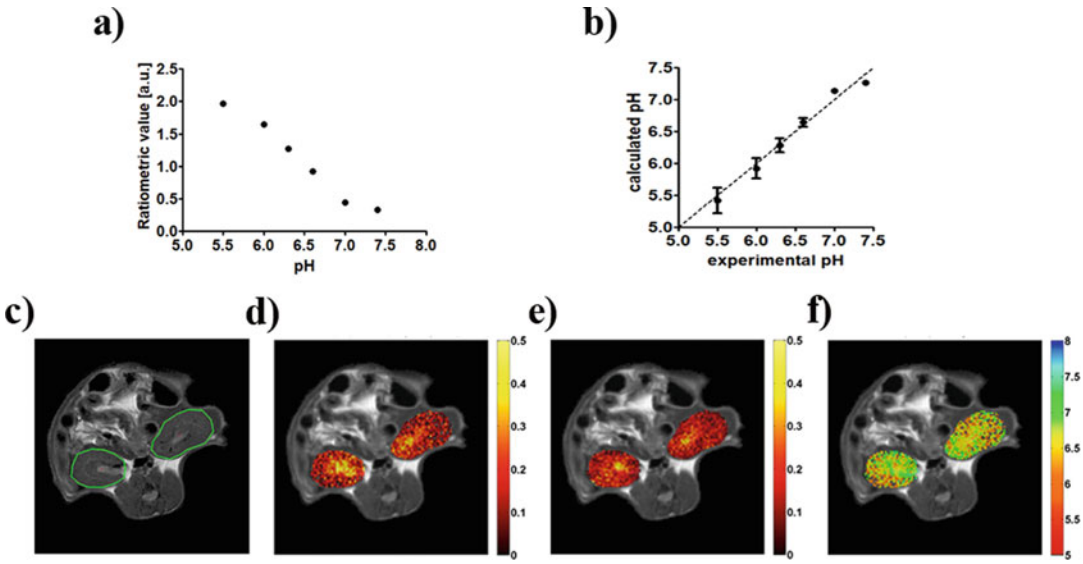

Fig. 2 Iopamidol ratiometric curve obtained from the rations of the CEST contrast upon irradiating at 4.2 and 5.5 ppm, respectively, showing the high pH responsiveness of Iopamidol. Irradiation power levels of 3 μT, Iopamidol 30 mM, 7.05 T, 310 K, irradiation time 5 s (**a**). Calculated pH values obtained by the ratiometric method (Iopamidol 30 mM, 7.05 T, 310 K, irradiation time 5 s, B_1 3 μT) are compared with the values read on the pH-meter (**b**). Representative images of in vivo renal pH mapping showing the anatomical image (**c**) and the CEST contrast parametric maps overlaid to the anatomical image at 4.2 ppm (**d**) and 5.5 ppm (**e**) and the observed pH map (**f**) obtained by ratioing maps (**d**) and (**e**) and using the calibration curve in (**a**) for calculating the pH values. (Adapted with permission from *Magnetic Resonance in Medicine* 2011 (Iopamidol as a responsive MRI-chemical exchange saturation transfer contrast agent for pH mapping of kidneys: in vivo studies in mice at 7 T. Volume: 65, Issue: 1, Pages: 202–211, DOI: https:/doi.org/10.1002/mrm.22608))

observed upon alkaline water administration. Both observations demonstrate the capability to measure in vivo renal pH changes with CEST MRI.

Since the accuracy in measuring pH depends on several factors, including chemical exchange rate, irradiation conditions (saturation power and duration), and main magnetic field, quantification of multisite pH-dependent chemical exchange properties is needed to improve pH accuracy [48]. This characterization of chemical exchange rates and optimal irradiation RF pulses led to the development of an optimized saturation for each single amide proton pools, hence resulting in a higher pH sensitivity. As a result, the capability to measure pH was demonstrated also at magnetic field strengths of 4.7 T, where amide resonances partially overlap. In the study of Wu and coworkers, they demonstrated an improved pH sensitivity, extending the pH detection range from 5.5 to 7.5, with high resolution pH maps of the kidneys in healthy rats (Fig. 3) [49]. More recently, the exploitation of the same ratiometric approach for measuring in vivo pH was also demonstrated at magnetic fields as low as 3 T, which still preserved good pH accuracy [50].

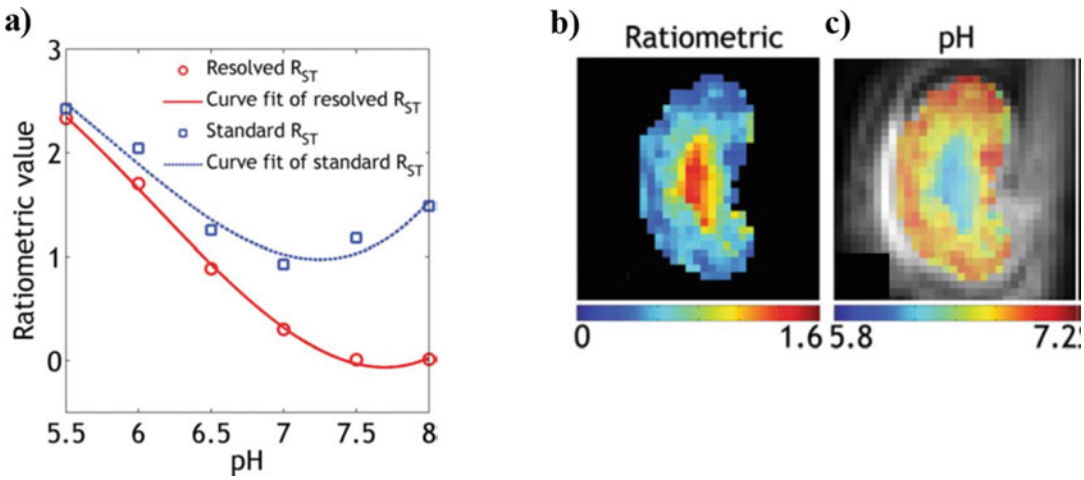

Fig. 3 Extension of pH detection range using the modified ratiometric analysis (red circles) versus the standard ratiometric approach (blue squares) (**a**). Representative in vivo ratiometric map for the proposed approach (**b**). pH map shows the renal pH gradually decreasing from the cortex, medulla to calyx (**c**). Maps are overlaid on the corresponding T_2-weighted image. (Adapted with permission from *Magnetic Resonance in Medicine* 2018 (A generalized ratiometric chemical exchange saturation transfer (CEST) MRI approach for mapping renal pH using Iopamidol, Volume: 79, Issue: 3, Pages: 1553–1558, DOI: https:/doi.org/10.1002/mrm.26817))

Another similar iodinated contrast media, Iopromide (Ultravist®, Bayer Healthcare, Germany), was also demonstrated and compared to Iopamidol for measuring pH, with a pH sensitivity that was not substantially different, although Iopamidol allows for more precise pH measurements [51].

The exploitation of the ratiometric approach requires two distinguishable protons pools on the same molecule, therefore it is limited to a select group of compounds possessing this feature. To overcome this limitation, Longo and Sun proposed a novel approach based on the irradiation of a single pool under different radiofrequency powers [52]. The proposed approach, called ratio of RF power mismatch or RPM, was demonstrated by using Iobitridol (Omnipaque®, GE Healthcare, USA), a radiographic contrast medium possessing only one amide proton pool resonating at 5.5 ppm (Fig. 1). Since the measured CEST contrast is dependent on both pH and irradiation power (B_1), a strong pH dependence was demonstrated by calculating the ratio of the CEST contrast at two different B_1 power levels. In comparison to the conventional ratiometric approach, a good pH accuracy and an even higher pH sensitivity were demonstrated. When investigated in healthy kidneys, the measured pH values upon iobitridol injection strongly correlated with the pH values obtained following iopamidol injection. Recently, to overcome the specific absorption rate (SAR) limitations when using a continuous wave (CW) irradiation of the mobile proton pools, a pulsed ratiometric approach has been

exploited and tested on the Iodixanol (Visipaque®, GE Healthcare, USA) X-ray contrast medium for CEST pH imaging [53].

Diamagnetic contrast agents possess resonances that are close in frequency to the bulk water signal resulting in a reduction of sensitivity (due to an inefficient labeling selectivity) when moving from high to low magnetic fields. Following previous investigations, McMahon and colleagues developed new diamagnetic systems based on the imidazole, salicylate or anthranilate moieties which possess mobile protons shifted very far from the bulk water peak [54–56]. In particular, candidate compounds derived from imidazole-4,5-dicarboxamides (#5 and #8, Fig. 1) show a CEST signal shifted up to 7.8 ppm upfield by exploiting the presence of intramolecular bond shifted hydrogens. Besides the large chemical shift, a good pH sensitivity and a high-water solubility made compound #**5** suitable as a pH sensor and so it has been tested in vivo [57]. pH imaging of the kidneys at 11.7 T resulted in average pH values for the whole kidneys of 6.5 ± 0.1, consistent with renal pH values reported by radiographic contrast agents (Fig. 4).

2.2.2 Paramagnetic CEST Agents

Paramagnetic chemical exchange saturation transfer (paraCEST) agents typically consist of a paramagnetic metal ion and an organic chelate based on a macrocyclic cage due to the high kinetic stability of these metal chelates to prevent the release of the toxic free lanthanide cation [58]. The CEST signal is therefore generated by selective irradiation of the bound water molecule, or of the slowly exchanging ligand protons, such as hydroxyl, amine, or amide groups [59–62]. The main advantage of paraCEST agents in comparison to diamagnetic ones relies in the exceptionally large chemical shifts (MR frequency relative to the water frequency) due to the hypershift contribution of the lanthanide metal ion. This large range of chemical shifts increases the specificity of the exchanging proton pools, hence reducing the adverse contributions of direct saturation and of the endogenous semisolid macromolecular effects [63]. Since the chemical exchange rate of the paraCEST agent can be altered by environmental factors such as pH, changes in CEST amplitudes can be used as well for deriving pH values.

The first demonstration of CEST detection in kidneys using a paraCEST agent (TmDOTA-4AmC, Fig. 1) was provided by Vinogradov et al., showing good detectability in the whole kidney regions [64]. Later on, a Europium paraCEST pH responsive agent (europium(III) DO3A-tris(amide) complex, Fig. 1) was exploited to measure pH in mouse kidneys [65]. Owing to its chemical structure, a quite large frequency shift of the ion-bound water molecule due to the delocalization of negative charge coming from deprotonation of phenolic residue was observed. This shift is pH dependent, therefore an alkalinisation from 6.0 to 7.6 at 298 K leads to a 4 ppm shift in frequencies, from 50.5 to

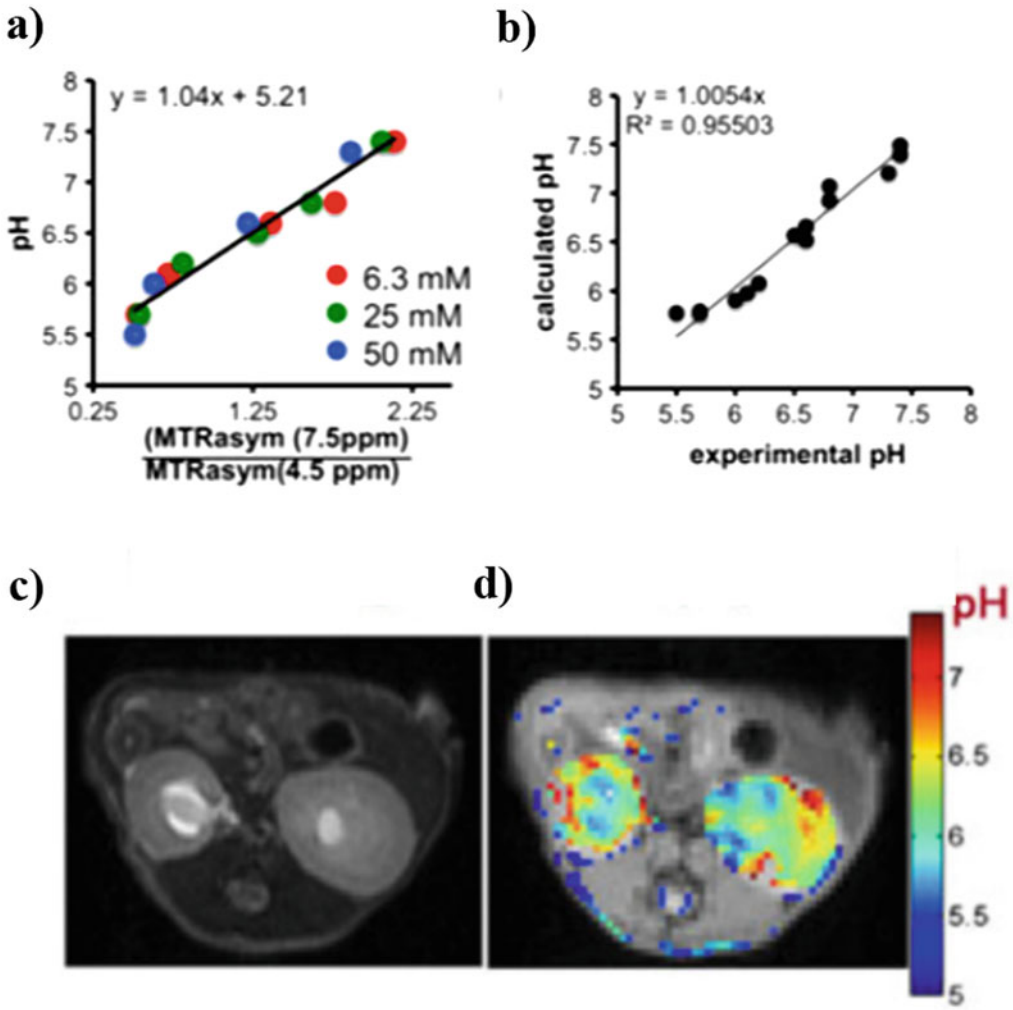

Fig. 4 pH calibration curve of compound #5 (**a**) and calibration plot using all tubes in the phantom showing experimental versus calculated pH (**b**). Experimental conditions: CEST data were obtained at 6.25 mM, 25 mM, or 50 mM concentration, saturation time = 3 s, saturation power = 5.9 μT and 37 °C. pH measurements were made with a precision of ±0.1 unit. T_2-weighted image (**c**) and pH map (**d**) following administration of compound #5. (Adapted with permission from *Contrast Media Molecular Imaging* 2016 (Developing imidazoles as CEST MRI pH sensors, Volume: 11, Issue: 4, Pages: 304–312, DOI: https:/doi.org/10.1002/cmmi.1693))

54.5 ppm, respectively, that can be exploited for assessing pH. By exploiting a 9.4 T MR scanner and ensuring stable temperature homogeneity, in vivo pH measurements were feasible in kidneys upon the administration of a dose of 0.4 mmol/kg [66].

2.3 Imaging Readout

CEST MRI techniques includes continuous wave (CW) or pulsed train RF saturation to prepare the magnetization followed by a fast image readout such as echo planar imaging (EPI), Rapid Imaging with Refocused Echoes (RARE) and/or fast imaging with steady-

state precession (FISP) [45, 67, 68]. More advanced methods now provide more sophisticated sampling schemes, such as 3D radial or spiral acquisitions, but those are currently available only on clinical scanners and not on preclinical scanners, thus limiting CEST acquisition in mice and rats to single slice based approaches [69, 70]. However, recent studies have utilized multislice acquisition schemes on preclinical scanners as well [67, 71, 72].

2.3.1 Rapid Imaging with Refocused Echoes (RARE)

Fast spin echo (FSE) or rapid imaging with refocused echoes (RARE) are commonly used because of the strong SNR (signal-to-noise ratio), high tolerance to B_0 inhomogeneities and moderate to short acquisition times. These methods allow acquisitions of several lines for full sampling the k-space for a single slice within a single TR, which greatly reduces the acquisition time and still preserves SNR. With single shot acquisitions, usually centric encoding is exploited to maximize the SNR. Further reductions in acquisition time can be achieved by adjusting the bandwidth (hence reducing the echo times or the distance between each refocused echo time) or by partial Fourier approaches (i.e., by acquiring only a portion of the k-space).

2.3.2 Fast Imaging with Steady-State Precession (FISP)

FISP readout has been used with CEST MRI that provides robust image readout with little distortion, although more sensitive to B_0 inhomogeneity than RARE. B_0 inhomogeneity might be an important issue particularly for body applications like the kidneys.

2.3.3 Spin-Echo Echo Planar Imaging (EPI)

CEST MRI is often combined with EPI acquisition, which provides fast image readout after a relatively long RF saturation. Whereas both gradient echo and spin echo EPI have been used, SE EPI is often preferred for body application because it is less susceptible to mild magnetic field inhomogeneity distortions that are common in body applications. The use of an EPI readout also enables multislice acquisitions in reasonable times.

3 Overview of Applications

CEST imaging has been exploited for assessing renal pH values in healthy and in several models of renal damage, including either bilateral or unilateral acute kidney injury models. Both endogenous CEST approaches and exogenous CEST approaches have been proposed and validated in vivo.

3.1 Endogenous CEST Methods for Assessing Renal Diseases

Since diabetic nephropathies (DNs) are associated with changes in renal metabolites, the utility of CEST MRI to detect changes in glucose/glycogen hydroxylic protons was investigated in murine models of diabetic nephropathies. The study was conducted longitudinally from 8 to 24 weeks on two groups of diabetic mice and on nondiabetic mice as control. Based on the variation of glucose/

glycogen composition and the consequent CEST effects measured in kidney regions, a significantly increased CEST of hydroxyl metabolites was observed in diabetic mice during the progression of DN [73].

3.2 CEST pH Imaging for Assessing Renal Diseases

Most of the studies reported so far have exploited the pH-responsiveness of Iopamidol for investigating the changes in pH homeostasis following renal injuries. In one of these studies, the pH evolution in an acute kidney injury model induced by intramuscular glycerol injection and consequent rhabdomyolysis was monitored [74]. Renal pH maps acquired at 1, 3, 7, 14, 21 days after the injury reported a marked increase of pH values during the damage evolution up to 3–7 days, followed by recovery of pH toward baseline values at 14 and 21 days. These results were in good agreement with morphological and Blood Urean Nitrogen (BUN) quantification supporting this CEST MRI pH mapping approach for investigating renal function. Furthermore, along with the progression of the damage, a reduction of pixels where Iopamidol was detectable was observed, suggesting that also the percentage of CEST-detected pixels can be used as an imaging biomarker of renal injury.

In another study, Longo and coworkers investigated a unilateral kidney ischemia reperfusion injury (KIRI) model to validate MRI-CEST pH mapping for assessing single kidney functionality [75]. Two different times of ischemia duration, 20 and 40 min, were applied to model moderate or severe KIRI, respectively. Following the damage evolution at days 0, 1, 2, 7, a significant increase in renal pH values was observed even at day 1 in both cases. Furthermore, in the following MRI acquisitions a clear distinction between moderate and severe AKI is possible since a recovery of normal acid-base balance was observed only in the moderate KIRI mice whereas in severe KIRI mice the increased pH values did not restore to baseline values (Fig. 5a, b). In additions, as in the previous study, the percentage of CEST detected pixels, representing a marker of the filtration fraction, showed significant differences between the injured kidneys and the contralateral ones, reflecting the different evolution of moderate-to-severe damage (Fig. 5c, d).

3.3 GlucoCEST Imaging for Assessing Renal Diseases

Since the capability of CEST imaging to detect hydroxyl protons, native glucose has also been proposed as a tracer for MRI GlucoCEST imaging [76–78]. Besides its exploitation in oncological applications, it has been applied for monitoring allograft rejection [79]. In this study, Brown Norway rat kidneys were transplanted into Lewis rats and imaged 4 days following the surgery, before and after glucose administration. By calculating the cortex-to-medulla CEST ratio (CESTR), dependent on the accumulation of the administered glucose, rats that underwent allogeneic transplant showed the highest CESTR values compared to syngeneic transplant group and to control mice.

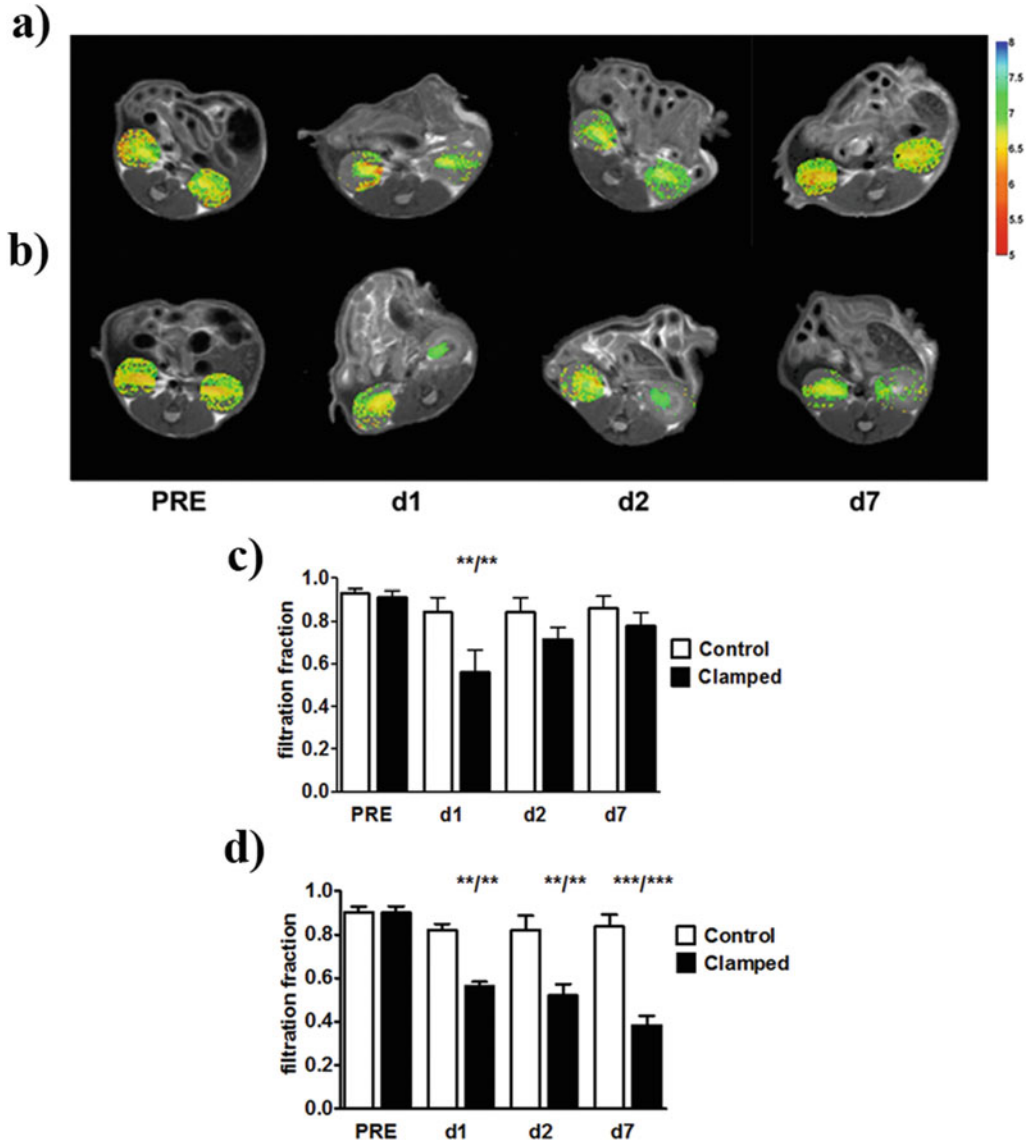

Fig. 5 MRI-CEST pH mapping detects renal pH changes and regional distribution of damage after moderate and severe unilateral kidney ischemia reperfusion injury (KIRI) showing clamped (right) and contralateral normal kidney (left). Representative MRI-CEST pH maps overimposed onto anatomical images before and after moderate (**a**) and severe (**b**) KIRI at different time points (day 1, day 2, and day 7) showing pronounced alkalinization and reduced filtration (noncolored pixels within the renal region, **c**, **d**) of the pH-responsive contrast agent in clamped kidney in comparison to contralateral kidney. (Adapted with permission from: *NMR in Biomedicine* 2017 (Noninvasive evaluation of renal pH homeostasis after ischemia reperfusion injury by CEST-MRI, Volume: 30, Issue: 7, DOI: https:/doi.org/10.1002/nbm.3720))

Acknowledgments

The Italian Ministry for Education and Research (MIUR) is gratefully acknowledged for yearly FOE funding to the Euro-BioImaging Multi-Modal Molecular Imaging Italian Node (MMMI).
This chapter is based upon work from COST Action PARENCHIMA, supported by European Cooperation in Science and Technology (COST). COST (www.cost.eu) is a funding agency for research and innovation networks. COST Actions help connect research initiatives across Europe and enable scientists to enrich their ideas by sharing them with their peers. This boosts their research, career, and innovation.
PARENCHIMA (renalmri.org) is a community-driven Action in the COST program of the European Union, which unites more than 200 experts in renal MRI from 30 countries with the aim to improve the reproducibility and standardization of renal MRI biomarkers.

References

1. Al Malla M, Varghese NV, AlAbdullatif M, Narchi H, Khassawneh M (2017) Prevalence and outcome of acute kidney injury, as defined by the new kidney disease improving global outcomes guideline, in very low birth weight infants. World J Nephrol 6(5):229–235. https://doi.org/10.5527/wjn.v6.i5.229
2. Kassebaum NJ, Lopez AD, Murray CJ, Lozano R (2014) A comparison of maternal mortality estimates from GBD 2013 and WHO. Lancet 384(9961):2209–2210. https://doi.org/10.1016/S0140-6736(14)62421-1
3. Zollner FG, Kalayciyan R, Chacon-Caldera J, Zimmer F, Schad LR (2014) Pre-clinical functional magnetic resonance imaging part I: the kidney. Z Med Phys 24(4):286–306. https://doi.org/10.1016/j.zemedi.2014.05.002
4. Neugarten J, Golestaneh L (2014) Blood oxygenation level-dependent MRI for assessment of renal oxygenation. Int J Nephrol Renovasc Dis 7:421–435. https://doi.org/10.2147/IJNRD.S42924
5. Zimmer F, Zollner FG, Hoeger S, Klotz S, Tsagogiorgas C, Kramer BK, Schad LR (2013) Quantitative renal perfusion measurements in a rat model of acute kidney injury at 3T: testing inter- and intramethodical significance of ASL and DCE-MRI. PLoS One 8(1): e53849. https://doi.org/10.1371/journal.pone.0053849
6. Ichikawa S, Motosugi U, Ichikawa T, Sano K, Morisaka H, Araki T (2013) Intravoxel incoherent motion imaging of the kidney: alterations in diffusion and perfusion in patients with renal dysfunction. Magn Reson Imaging 31 (3):414–417. https://doi.org/10.1016/j.mri.2012.08.004
7. Clatworthy MR, Kettunen MI, Hu DE, Mathews RJ, Witney TH, Kennedy BW, Bohndiek SE, Gallagher FA, Jarvis LB, Smith KG, Brindle KM (2012) Magnetic resonance imaging with hyperpolarized [1,4-(13)C2]fumarate allows detection of early renal acute tubular necrosis. Proc Natl Acad Sci U S A 109 (33):13374–13379. https://doi.org/10.1073/pnas.1205539109
8. Warner L, Yin M, Glaser KJ, Woollard JA, Carrascal CA, Korsmo MJ, Crane JA, Ehman RL, Lerman LO (2011) Noninvasive in vivo assessment of renal tissue elasticity during graded renal ischemia using MR elastography. Investig Radiol 46(8):509–514. https://doi.org/10.1097/RLI.0b013e3182183a95
9. Oostendorp M, de Vries EE, Slenter JM, Peutz-Kootstra CJ, Snoeijs MG, Post MJ, van Heurn LW, Backes WH (2011) MRI of renal oxygenation and function after normothermic ischemia-reperfusion injury. NMR Biomed 24 (2):194–200. https://doi.org/10.1002/nbm.1572

10. Notohamiprodjo M, Reiser MF, Sourbron SP (2010) Diffusion and perfusion of the kidney. Eur J Radiol 76(3):337–347. https://doi.org/10.1016/j.ejrad.2010.05.033
11. Prasad PV (2006) Evaluation of intra-renal oxygenation by BOLD MRI. Nephron Clin Pract 103(2):c58–c65. https://doi.org/10.1159/000090610
12. Kline TL, Edwards ME, Garg I, Irazabal MV, Korfiatis P, Harris PC, King BF, Torres VE, Venkatesh SK, Erickson BJ (2018) Quantitative MRI of kidneys in renal disease. Abdom Radiol (NY) 43(3):629–638. https://doi.org/10.1007/s00261-017-1236-y
13. Zhang JL, Morrell G, Rusinek H, Sigmund EE, Chandarana H, Lerman LO, Prasad PV, Niles D, Artz N, Fain S, Vivier PH, Cheung AK, Lee VS (2014) New magnetic resonance imaging methods in nephrology. Kidney Int 85(4):768–778. https://doi.org/10.1038/ki.2013.361
14. Zhang JL, Rusinek H, Chandarana H, Lee VS (2013) Functional MRI of the kidneys. J Magn Reson Imaging 37(2):282–293. https://doi.org/10.1002/jmri.23717
15. Grenier N, Pedersen M, Hauger O (2006) Contrast agents for functional and cellular MRI of the kidney. Eur J Radiol 60(3):341–352. https://doi.org/10.1016/j.ejrad.2006.06.024
16. Liu G, Song X, Chan KW, McMahon MT (2013) Nuts and bolts of chemical exchange saturation transfer MRI. NMR Biomed 26(7):810–828. https://doi.org/10.1002/nbm.2899
17. Kogan F, Hariharan H, Reddy R (2013) Chemical exchange saturation transfer (CEST) imaging: description of technique and potential clinical applications. Curr Radiol Rep 1(2):102–114. https://doi.org/10.1007/s40134-013-0010-3
18. Jones KM, Pollard AC, Pagel MD (2018) Clinical applications of chemical exchange saturation transfer (CEST) MRI. J Magn Reson Imaging 47(1):11–27. https://doi.org/10.1002/jmri.25838
19. Anemone A, Consolino L, Arena F, Capozza M, Longo DL (2019) Imaging tumor acidosis: a survey of the available techniques for mapping in vivo tumor pH. Cancer Metastasis Rev 38(1-2):25–49. https://doi.org/10.1007/s10555-019-09782-9
20. Ward KM, Aletras AH, Balaban RS (2000) A new class of contrast agents for MRI based on proton chemical exchange dependent saturation transfer (CEST). J Magn Reson 143(1):79–87. https://doi.org/10.1006/jmre.1999.1956
21. Sun PZ, Benner T, Copen WA, Sorensen AG (2010) Early experience of translating pH-weighted MRI to image human subjects at 3 Tesla. Stroke 41(10 Suppl):S147–S151. https://doi.org/10.1161/STROKEAHA.110.595777
22. Aime S, Castelli DD, Crich SG, Gianolio E, Terreno E (2009) Pushing the sensitivity envelope of lanthanide-based magnetic resonance imaging (MRI) contrast agents for molecular imaging applications. Acc Chem Res 42(7):822–831. https://doi.org/10.1021/ar800192p
23. McMahon MT, Gilad AA, DeLiso MA, Berman SM, Bulte JW, van Zijl PC (2008) New "multicolor" polypeptide diamagnetic chemical exchange saturation transfer (DIACEST) contrast agents for MRI. Magn Reson Med 60(4):803–812. https://doi.org/10.1002/mrm.21683
24. Sun PZ, Zhou J, Huang J, van Zijl P (2007) Simplified quantitative description of amide proton transfer (APT) imaging during acute ischemia. Magn Reson Med 57(2):405–410. https://doi.org/10.1002/mrm.21151
25. McMahon MT, Gilad AA, Zhou J, Sun PZ, Bulte JW, van Zijl PC (2006) Quantifying exchange rates in chemical exchange saturation transfer agents using the saturation time and saturation power dependencies of the magnetization transfer effect on the magnetic resonance imaging signal (QUEST and QUESP): Ph calibration for poly-L-lysine and a starburst dendrimer. Magn Reson Med 55(4):836–847. https://doi.org/10.1002/mrm.20818
26. Jones CK, Schlosser MJ, van Zijl PC, Pomper MG, Golay X, Zhou J (2006) Amide proton transfer imaging of human brain tumors at 3T. Magn Reson Med 56(3):585–592. https://doi.org/10.1002/mrm.20989
27. Sun PZ, Wang E, Cheung JS (2012) Imaging acute ischemic tissue acidosis with pH-sensitive endogenous amide proton transfer (APT) MRI--correction of tissue relaxation and concomitant RF irradiation effects toward mapping quantitative cerebral tissue pH. NeuroImage 60(1):1–6. https://doi.org/10.1016/j.neuroimage.2011.11.091
28. Haris M, Nath K, Cai K, Singh A, Crescenzi R, Kogan F, Verma G, Reddy S, Hariharan H, Melhem ER, Reddy R (2013) Imaging of glutamate neurotransmitter alterations in Alzheimer's disease. NMR Biomed 26(4):386–391. https://doi.org/10.1002/nbm.2875
29. Longo DL, Di Gregorio E, Abategiovanni R, Ceccon A, Assfalg M, Molinari H, Aime S

(2014) Chemical exchange saturation transfer (CEST): an efficient tool for detecting molecular information on proteins' behaviour. Analyst 139(11):2687–2690. https://doi.org/10.1039/c4an00346b

30. Ceccon A, D'Onofrio M, Zanzoni S, Longo DL, Aime S, Molinari H, Assfalg M (2013) NMR investigation of the equilibrium partitioning of a water-soluble bile salt protein carrier to phospholipid vesicles. Proteins 81 (10):1776–1791. https://doi.org/10.1002/prot.24329
31. Castelli DD, Terreno E, Longo D, Aime S (2013) Nanoparticle-based chemical exchange saturation transfer (CEST) agents. NMR Biomed 26(7):839–849. https://doi.org/10.1002/nbm.2974
32. Dastru W, Longo D, Aime S (2011) Contrast agents and mechanisms. Drug Discov Today 8 (2–4):e109–e115. https://doi.org/10.1016/j.ddtec.2011.11.013
33. Sherry AD, Woods M (2008) Chemical exchange saturation transfer contrast agents for magnetic resonance imaging. Annu Rev Biomed Eng 10:391–411. https://doi.org/10.1146/annurev.bioeng.9.060906.151929
34. Zaiss M, Windschuh J, Goerke S, Paech D, Meissner JE, Burth S, Kickingereder P, Wick W, Bendszus M, Schlemmer HP, Ladd ME, Bachert P, Radbruch A (2016) Downfield-NOE-suppressed amide-CEST-MRI at 7 Tesla provides a unique contrast in human glioblastoma. Magn Reson Med 77 (1):196–208. https://doi.org/10.1002/mrm.26100
35. Rivlin M, Navon G (2016) Glucosamine and N-acetyl glucosamine as new CEST MRI agents for molecular imaging of tumors. Sci Rep 6:32648. https://doi.org/10.1038/srep32648
36. Li Y, Chen H, Xu J, Yadav NN, Chan KW, Luo L, McMahon MT, Vogelstein B, van Zijl PC, Zhou S, Liu G (2016) CEST theranostics: label-free MR imaging of anticancer drugs. Oncotarget 7(6):6369–6378. https://doi.org/10.18632/oncotarget.7141
37. Desmond KL, Mehrabian H, Chavez S, Sahgal A, Soliman H, Rola R, Stanisz GJ (2017) Chemical exchange saturation transfer for predicting response to stereotactic radiosurgery in human brain metastasis. Magn Reson Med 78(3):1110–1120. https://doi.org/10.1002/mrm.26470
38. Goerke S, Breitling J, Zaiss M, Windschuh J, Kunz P, Schuenke P, Paech D, Longo DL, Klika KD, Ladd ME, Bachert P (2018) Dual-frequency irradiation CEST-MRI of endogenous bulk mobile proteins. NMR Biomed 31 (6):e3920. https://doi.org/10.1002/nbm.3920
39. Longo DL, Moustaghfir FZ, Zerbo A, Consolino L, Anemone A, Bracesco M, Aime S (2017) EXCI-CEST: exploiting pharmaceutical excipients as MRI-CEST contrast agents for tumor imaging. Int J Pharm 525 (1):275–281. https://doi.org/10.1016/j.ijpharm.2017.04.040
40. Ward KM, Balaban RS (2000) Determination of pH using water protons and chemical exchange dependent saturation transfer (CEST). Magn Reson Med 44(5):799–802. https://doi.org/10.1002/1522-2594
41. Longo D, Aime S (2017) Iodinated contrast media as pH-responsive CEST agents. In: McMahon MT, Gilad AA, Bulte JBM, Van Zijl PCM (eds) Chemical exchange saturation transfer imaging, Advances and applications. Pan Stanford Publishing, Singapore, pp 447–466. https://doi.org/10.1201/9781315364421-20
42. McDonald RJ, McDonald JS, Bida JP, Carter RE, Fleming CJ, Misra S, Williamson EE, Kallmes DF (2013) Intravenous contrast material-induced nephropathy: causal or coincident phenomenon? Radiology 267 (1):106–118. https://doi.org/10.1148/radiol.12121823
43. McDonald JS, McDonald RJ, Comin J, Williamson EE, Katzberg RW, Murad MH, Kallmes DF (2013) Frequency of acute kidney injury following intravenous contrast medium administration: a systematic review and meta-analysis. Radiology 267(1):119–128. https://doi.org/10.1148/radiol.12121460
44. Aime S, Calabi L, Biondi L, De Miranda M, Ghelli S, Paleari L, Rebaudengo C, Terreno E (2005) Iopamidol: exploring the potential use of a well-established x-ray contrast agent for MRI. Magn Reson Med 53(4):830–834. https://doi.org/10.1002/mrm.20441
45. Longo DL, Dastru W, Digilio G, Keupp J, Langereis S, Lanzardo S, Prestigio S, Steinbach O, Terreno E, Uggeri F, Aime S (2011) Iopamidol as a responsive MRI-chemical exchange saturation transfer contrast agent for pH mapping of kidneys: in vivo studies in mice at 7 T. Magn Reson Med 65(1):202–211. https://doi.org/10.1002/mrm.22608
46. Anemone A, Consolino L, Longo DL (2017) MRI-CEST assessment of tumour perfusion using X-ray iodinated agents: comparison with a conventional Gd-based agent. Eur Radiol 27 (5):2170–2179. https://doi.org/10.1007/s00330-016-4552-7
47. Longo DL, Michelotti F, Consolino L, Bardini P, Digilio G, Xiao G, Sun PZ, Aime S

(2016) In vitro and in vivo assessment of non-ionic iodinated radiographic molecules as chemical exchange saturation transfer magnetic resonance imaging tumor perfusion agents. Investig Radiol 51(3):155–162. https://doi.org/10.1097/RLI.0000000000000217

48. Sun PZ, Longo DL, Hu W, Xiao G, Wu R (2014) Quantification of iopamidol multi-site chemical exchange properties for ratiometric chemical exchange saturation transfer (CEST) imaging of pH. Phys Med Biol 59 (16):4493–4504. https://doi.org/10.1088/0031-9155/59/16/4493
49. Wu Y, Zhou IY, Igarashi T, Longo DL, Aime S, Sun PZ (2018) A generalized ratiometric chemical exchange saturation transfer (CEST) MRI approach for mapping renal pH using iopamidol. Magn Reson Med 79 (3):1553–1558. https://doi.org/10.1002/mrm.26817
50. Longo DL, Bartoli A, Consolino L, Bardini P, Arena F, Schwaiger M, Aime S (2016) In vivo imaging of tumor metabolism and acidosis by combining PET and MRI-CEST pH imaging. Cancer Res 76(22):6463–6470. https://doi.org/10.1158/0008-5472.CAN-16-0825
51. Moon BF, Jones KM, Chen LQ, Liu P, Randtke EA, Howison CM, Pagel MD (2015) A comparison of iopromide and iopamidol, two acidoCEST MRI contrast media that measure tumor extracellular pH. Contrast Media Mol Imaging 10(6):446–455. https://doi.org/10.1002/cmmi.1647
52. Longo DL, Sun PZ, Consolino L, Michelotti FC, Uggeri F, Aime S (2014) A general MRI-CEST ratiometric approach for pH imaging: demonstration of in vivo pH mapping with iobitridol. J Am Chem Soc 136 (41):14333–14336. https://doi.org/10.1021/ja5059313
53. Arena F, Irrera P, Consolino L, Colombo Serra S, Zaiss M, Longo DL (2018) Flip-angle based ratiometric approach for pulsed CEST-MRI pH imaging. J Magn Reson 287:1–9. https://doi.org/10.1016/j.jmr.2017.12.007
54. Song X, Walczak P, He X, Yang X, Pearl M, Bulte JW, Pomper MG, McMahon MT, Janowski M (2016) Salicylic acid analogues as chemical exchange saturation transfer MRI contrast agents for the assessment of brain perfusion territory and blood-brain barrier opening after intra-arterial infusion. J Cereb Blood Flow Metab 36(7):1186–1194. https://doi.org/10.1177/0271678X16637882
55. Song X, Yang X, Ray Banerjee S, Pomper MG, McMahon MT (2015) Anthranilic acid analogs as diamagnetic CEST MRI contrast agents that feature an intramolecular-bond shifted hydrogen. Contrast Media Mol Imaging 10 (1):74–80. https://doi.org/10.1002/cmmi.1597
56. Yang X, Song X, Li Y, Liu G, Ray Banerjee S, Pomper MG, McMahon MT (2013) Salicylic acid and analogues as diaCEST MRI contrast agents with highly shifted exchangeable proton frequencies. Angew Chem Int Ed Engl 52 (31):8116–8119. https://doi.org/10.1002/anie.201302764
57. Yang X, Song X, Ray Banerjee S, Li Y, Byun Y, Liu G, Bhujwalla ZM, Pomper MG, McMahon MT (2016) Developing imidazoles as CEST MRI pH sensors. Contrast Media Mol Imaging 11(4):304–312. https://doi.org/10.1002/cmmi.1693
58. Zhang S, Merritt M, Woessner DE, Lenkinski RE, Sherry AD (2003) PARACEST agents: modulating MRI contrast via water proton exchange. Acc Chem Res 36(10):783–790. https://doi.org/10.1021/ar020228m
59. Hancu I, Dixon WT, Woods M, Vinogradov E, Sherry AD, Lenkinski RE (2010) CEST and PARACEST MR contrast agents. Acta Radiol 51(8):910–923. https://doi.org/10.3109/02841851.2010.502126
60. Liu G, Ali MM, Yoo B, Griswold MA, Tkach JA, Pagel MD (2009) PARACEST MRI with improved temporal resolution. Magn Reson Med 61(2):399–408. https://doi.org/10.1002/mrm.21863
61. Aime S, Delli Castelli D, Terreno E (2005) Highly sensitive MRI chemical exchange saturation transfer agents using liposomes. Angew Chem Int Ed Engl 44(34):5513–5515. https://doi.org/10.1002/anie.200501473
62. Srivastava K, Ferrauto G, Harris SM, Longo DL, Botta M, Aime S, Pierre VC (2018) Complete on/off responsive ParaCEST MRI contrast agents for copper and zinc. Dalton Trans 47(33):11346–11357. https://doi.org/10.1039/c8dt01172a
63. Woods M, Woessner DE, Sherry AD (2006) Paramagnetic lanthanide complexes as PARACEST agents for medical imaging. Chem Soc Rev 35(6):500–511. https://doi.org/10.1039/b509907m
64. Vinogradov E, He H, Lubag A, Balschi JA, Sherry AD, Lenkinski RE (2007) MRI detection of paramagnetic chemical exchange effects in mice kidneys in vivo. Magn Reson Med 58 (4):650–655. https://doi.org/10.1002/mrm.21393
65. Wu Y, Soesbe TC, Kiefer GE, Zhao P, Sherry AD (2010) A responsive europium(III) chelate that provides a direct readout of pH by MRI. J Am Chem Soc 132(40):14002–14003. https://doi.org/10.1021/ja106018n

66. Wu Y, Zhang S, Soesbe TC, Yu J, Vinogradov E, Lenkinski RE, Sherry AD (2016) pH imaging of mouse kidneys in vivo using a frequency-dependent paraCEST agent. Magn Reson Med 75(6):2432–2441. https://doi.org/10.1002/mrm.25844
67. Sun PZ, Cheung JS, Wang E, Benner T, Sorensen AG (2011) Fast multislice pH-weighted chemical exchange saturation transfer (CEST) MRI with unevenly segmented RF irradiation. Magn Reson Med 65(2):588–594. https://doi.org/10.1002/mrm.22628
68. Sheth VR, Li Y, Chen LQ, Howison CM, Flask CA, Pagel MD (2012) Measuring in vivo tumor pHe with CEST-FISP MRI. Magn Reson Med 67(3):760–768. https://doi.org/10.1002/mrm.23038
69. Zaiss M, Ehses P, Scheffler K (2018) Snapshot-CEST: optimizing spiral-centric-reordered gradient echo acquisition for fast and robust 3D CEST MRI at 9.4 T. NMR Biomed 31(4):e3879. https://doi.org/10.1002/nbm.3879
70. Zhu H, Jones CK, van Zijl PC, Barker PB, Zhou J (2010) Fast 3D chemical exchange saturation transfer (CEST) imaging of the human brain. Magn Reson Med 64(3):638–644. https://doi.org/10.1002/mrm.22546
71. Sun PZ, Murata Y, Lu J, Wang X, Lo EH, Sorensen AG (2008) Relaxation-compensated fast multislice amide proton transfer (APT) imaging of acute ischemic stroke. Magn Reson Med 59(5):1175–1182. https://doi.org/10.1002/mrm.21591
72. Randtke EA, Granados JC, Howison CM, Pagel MD, Cardenas-Rodriguez J (2017) Multislice CEST MRI improves the spatial assessment of tumor pH. Magn Reson Med 78(1):97–106. https://doi.org/10.1002/mrm.26348
73. Wang F, Kopylov D, Zu Z, Takahashi K, Wang S, Quarles CC, Gore JC, Harris RC, Takahashi T (2016) Mapping murine diabetic kidney disease using chemical exchange saturation transfer MRI. Magn Reson Med 76(5):1531–1541. https://doi.org/10.1002/mrm.26045
74. Longo DL, Busato A, Lanzardo S, Antico F, Aime S (2013) Imaging the pH evolution of an acute kidney injury model by means of iopamidol, a MRI-CEST pH-responsive contrast agent. Magn Reson Med 70(3):859–864. https://doi.org/10.1002/mrm.24513
75. Longo DL, Cutrin JC, Michelotti F, Irrera P, Aime S (2017) Noninvasive evaluation of renal pH homeostasis after ischemia reperfusion injury by CEST-MRI. NMR Biomed 30(7). https://doi.org/10.1002/nbm.3720
76. Walker-Samuel S, Ramasawmy R, Torrealdea F, Rega M, Rajkumar V, Johnson SP, Richardson S, Goncalves M, Parkes HG, Arstad E, Thomas DL, Pedley RB, Lythgoe MF, Golay X (2013) In vivo imaging of glucose uptake and metabolism in tumors. Nat Med 19(8):1067–1072. https://doi.org/10.1038/nm.3252
77. Xu X, Chan KW, Knutsson L, Artemov D, Xu J, Liu G, Kato Y, Lal B, Laterra J, McMahon MT, van Zijl PC (2015) Dynamic glucose enhanced (DGE) MRI for combined imaging of blood-brain barrier break down and increased blood volume in brain cancer. Magn Reson Med 74(6):1556–1563. https://doi.org/10.1002/mrm.25995
78. Chan KW, McMahon MT, Kato Y, Liu G, Bulte JW, Bhujwalla ZM, Artemov D, van Zijl PC (2012) Natural D-glucose as a biodegradable MRI contrast agent for detecting cancer. Magn Reson Med 68(6):1764–1773. https://doi.org/10.1002/mrm.24520
79. Kentrup D, Bovenkamp P, Busch A, Schuette-Nuetgen K, Pawelski H, Pavenstadt H, Schlatter E, Herrmann KH, Reichenbach JR, Loffler B, Heitplatz B, Van Marck V, Yadav NN, Liu G, van Zijl PCM, Reuter S, Hoerr V (2017) GlucoCEST magnetic resonance imaging in vivo may be diagnostic of acute renal allograft rejection. Kidney Int 92(3):757–764. https://doi.org/10.1016/j.kint.2017.04.015

Open Access This chapter is licensed under the terms of the Creative Commons Attribution 4.0 International License (http://creativecommons.org/licenses/by/4.0/), which permits use, sharing, adaptation, distribution and reproduction in any medium or format, as long as you give appropriate credit to the original author(s) and the source, provide a link to the Creative Commons license and indicate if changes were made.

The images or other third party material in this chapter are included in the chapter's Creative Commons license, unless indicated otherwise in a credit line to the material. If material is not included in the chapter's Creative Commons license and your intended use is not permitted by statutory regulation or exceeds the permitted use, you will need to obtain permission directly from the copyright holder.